International Journal for Multidisciplinary Research (IJFMR)
E-ISSN: 2582-2160 ● Website: www.ijfmr.com ● Email: editor@ijfmr.com

# Magnetic Insights: Unravelling Foetal and Placental Mysteries With MRI

**Dr. Bhawana Sonawane[1], Dr. Anagha Deshpande[2], Dr. Charu Bilaiya[3]**

[1]Prof and HOD, Radiodiagnosis
[2]Associate Professor, Radiodiagnosis
[3]Resident, Radiodiagnosis

**Abstract**

**Objective:** To evaluate the role of prenatal magnetic resonance imaging (MRI) in the detection and characterization of fetal and placental abnormalities when ultrasonography is inconclusive or limited.

**Methods:** This retrospective observational study was conducted at a tertiary care teaching hospital between January 2020 and March 2025. Pregnant women referred for foetal MRI due to suspected congenital anomalies or placental pathology were included. MRI examinations were performed using standard foetal protocols, and abnormalities were categorized system-wise.

**Results:** Prenatal MRI enabled detailed assessment of central nervous system, thoracic, urogenital, musculoskeletal, and placental abnormalities. MRI provided superior delineation of cortical maturation, posterior fossa malformations, airway obstruction syndromes, pulmonary lesions, urinary tract anomalies, and placental invasion disorders. Several cases demonstrated associated multisystem anomalies that were not fully characterized on ultrasonography.

**Conclusion:** Prenatal MRI is a valuable complementary imaging modality to ultrasonography, improving diagnostic accuracy and aiding clinical decision-making in complex fetal and placental abnormalities.

## Introduction

Prenatal imaging plays a critical role in the early detection of foetal and placental abnormalities, enabling timely clinical decision-making and improving perinatal outcomes. Ultrasonography (USG) remains the first-line imaging modality due to its wide availability, real-time capability, and cost-effectiveness. However, its diagnostic accuracy may be compromised in conditions such as maternal obesity, oligohydramnios, unfavourable foetal position, or complex congenital anomalies.

Magnetic resonance imaging (MRI) has gained increasing acceptance as a complementary modality in prenatal diagnosis. MRI provides excellent soft-tissue contrast, multiplanar visualization, and a large field of view without exposure to ionizing radiation.

These advantages make foetal MRI particularly useful for detailed assessment of the central nervous system (CNS), thoracic structures, abdominal organs, and placental pathologies. This study aims to illustrate the spectrum of foetal and placental abnormalities detected on prenatal MRI and highlight its growing role in comprehensive prenatal evaluation.

## Materials and Method:

This was a retrospective observational study conducted at a tertiary care referral centre in the Departme-

nt of Radiology over a five-year period from January 2020 to March 2025 on foetal MRI scans of 78 pregnant individuals referred for further evaluation of suspected anomalies . MRI findings were reviewed and categorized into normal and abnormal, with further classification of the type and location of anomalies. Cases with placental abnormalities were also documented.

**Inclusion Criteria**

- Patient gives informed consent
- Gestational age ≥18 weeks
- Age between 20 and 35 years
- Suspected foetal or placental abnormality on ultrasonography

**Exclusion Criteria**

- **Refusal to give informed consent**

The research was carried out in line with the Declaration of Helsinki and received ethical approval from the institution's ethics committee. During the initial appointment, the patient was asked to give written consent in their native language before undergoing a thorough history-taking and complete clinical examination. A thorough evaluation was conducted, which included information about the mother's age, previous pregnancies, estimated gestational age from the last menstrual period, menstrual cycle history, obstetric history, any past or current medical conditions, surgical history, medication use or allergies, smoking habits, alcohol consumption, and tobacco use. A comprehensive clinical assessment was conducted, which included checking blood pressure, body mass index (which is calculated as body weight in kilograms divided by the square of body height in meters), and a general survey evaluation.

*MRI data acquisition*

Pregnant patients were scanned using a 3T MRI system (Siemens). Patients were positioned in supine position. No sedation or contrast medium was given. A multichannel phased array body coil was used. Standard protocols included both T1-weighted and T2-weighted imaging, HASTE, sequences to assess foetal brain, heart, abdomen, musculoskeletal system, and placenta. Additional sequences such as diffusion-weighted imaging (DWI) were utilized for specific cases requiring further soft tissue characterization. Motion artifact reduction techniques were applied to ensure optimal image quality.

| Parameter | Details |
|---|---|
| Scanner | 3 T MRI system |
| Patient Position | Supine |
| Sequences Used | T1-weighted sequences<br>T2-weighted single-shot fast spin echo (HASTE)<br>Diffusion-weighted imaging (select cases) |
| Imaging Planes | Axial, coronal, sagittal |
| Slice Thickness | 3–5 mm |
| Sedation | None |

**Statistical analysis**

The data gathered was inputted into the Microsoft Excel spreadsheet designed for Windows 10. Statistical Package for the Social Sciences Version 22.0 (SPSS Inc., Chicago, Illinois, USA) software

was utilized for the analysis of the collected data. Following statistical analysis, the results were displayed in tables. Quantitative data were represented in numbers and percentages (%). Quantitative data were presented as mean ± SD.

The detection rates of foetal and placental abnormalities on ultrasonography and prenatal MRI were calculated. The incremental diagnostic yield of MRI over ultrasonography was assessed by identifying additional anomalies detected exclusively on MRI and cases in which MRI refined or altered the initial sonographic diagnosis. System-wise distribution of abnormalities was analyzed for central nervous system, thoracic, genitourinary, musculoskeletal, and placental pathologies.

Sensitivity, specificity, positive predictive value, and negative predictive value were not calculated, as uniform postnatal or pathological confirmation was not available for all cases, precluding the use of a definitive reference standard.

**Results:**

Out of the 78 foetal MRI cases, abnormalities were identified in 62 (79.5%) foetuses. Among these, 29 cases (46.8%) exhibited CNS anomalies such as ventriculomegaly, agenesis of the corpus callosum, and neural tube defects. Fifteen cases (24.2%) involved genitourinary tract anomalies including hydronephrosis, renal agenesis, and bladder outlet obstruction. Additionally, 11 cases (14.1%) demonstrated placental abnormalities, such as accreta spectrum disorders.

**Table 1 Maternal and Pregnancy Characteristics of the Study Population (n = 78)**

| **Parameter** | **Value** |
|---|---|
| Maternal age range(years) | 20-35 years |
| Gestational age at MRI range (weeks) | 18-24 weeks |
| Indication for MRI – suspected foetal anomaly | 85.8 % |
| Indication for MRI – suspected placental abnormality | 14.1 % |
| Singleton pregnancies | 98.70 % |
| Twin pregnancies | 1.28 % |

**Table 2. Overall Distribution of Foetal and Placental MRI Findings**

| MRI Finding | Number of Cases (n) | Percentage (%) |
|---|---|---|
| Normal MRI | **16** | **20.5** |
| Abnormal MRI | **62** | **79.5** |
| CNS anomalies | **29** | **46.8** |
| Genitourinary anomalies | **15** | **24.2** |
| Thoracic anomalies | **3** | **0.03** |
| Placental abnormalities | **11** | **14.1** |

**Table 3. Spectrum of Central Nervous System Abnormalities Detected on Fetal MRI (n = 29)**

| **CNS anomaly** | **No. of cases** |
|---|---|
| Colpocephaly (isolated or associated) | **7** |

| | |
|---|---|
| Agenesis/dysgenesis of corpus callosum | **6** |
| Dandy–Walker spectrum | **3** |
| Chiari II malformation | **4** |
| Holoprosencephaly (semilobar/lobar) | **3** |
| Encephalocele | **2** |
| Hydrocephalus | **4** |

**Table 4. Genitourinary anomalies identified on fetal MRI (n= 15)**

| Genitourinary anomaly | **No. of cases** |
|---|---|
| Multicystic dysplastic kidney (unilateral/bilateral/ectopic) | **3** |
| Renal agenesis (unilateral or bilateral) | **3** |
| Hydroureteronephrosis / PUJ obstruction | **2** |
| Urinary bladder outlet obstruction / megacystis | **2** |
| Ectopic / malrotated kidney | **3** |
| Vesicoureteric junction obstruction | **1** |
| Bilateral renal pyelectasis | **1** |

MRI was particularly useful in cases complicated by severe oligohydramnios where ultrasonography was limited.

**Table 5. Placental abnormalities detected on prenatal MRI**

| **Placental abnormality** | **Number of cases** |
|---|---|
| Placenta accreta / increta spectrum | **4** |
| Complete placenta previa | **3** |
| Marginal / low-lying placenta | **2** |
| Placental chorioangioma | **1** |
| Intraplacental / retroplacental hemorrhage | **1** |

Placenta accreta spectrum disorders showed typical MRI features including heterogeneous placental signal, intraplacental T2 hypointense bands, and loss of the retroplacental clear zone.

**Table 6. Added diagnostic value of fetal MRI compared with ultrasonography**

| **Organ system** | **Limitation of ultrasonography** | **Added value of MRI** |
|---|---|---|
| CNS | Limited sulcation and commissural evaluation | Cortical maturation, corpus callosal anatomy, posterior fossa assessment |
| Genitourinary | Poor visualization in oligohydramnios | Renal morphology, bladder outlet obstruction, ureteric dilatation |
| Thorax | Inadequate airway and lung assessment | Lung signal characterization, airway patency, mediastinal shift |
| Placenta | Uncertain depth of invasion | Accurate characterization of |

| | | |
|---|---|---|
| | | placental invasion |

**Interpretation of fetal MRI**

**NORMAL FETAL CNS ANATOMY:**

**Normal brain – at 23 weeks show multi-layered pattern that is normally observed until approximately 28 Wks.**

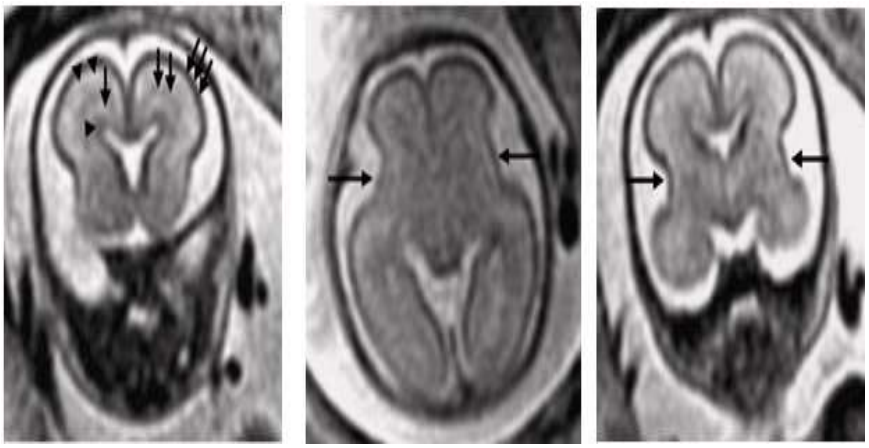

**Figure 1 Normal foetal cerebral cortical development.**

Axial and coronal T2-weighted images at 23 weeks' gestation demonstrate the normal multilayered appearance of the fetal cerebral parenchyma. The germinal matrix, periventricular zone, subventricular/intermediate zone, subplate, and developing cortex are distinctly visualized. Sylvian fissures appear angled and shallow, consistent with normal gestational age–appropriate brain maturation.

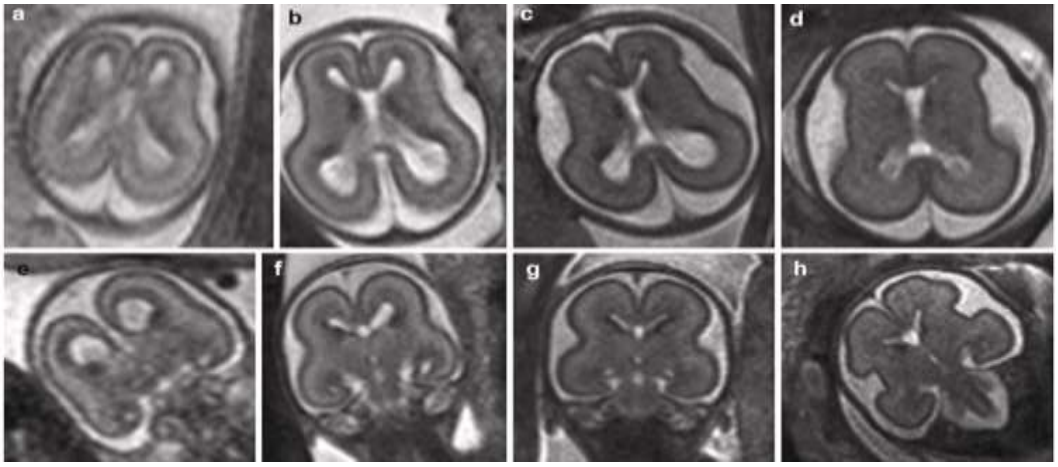


**Figure 2 Normal evolution of fetal brain parenchyma with advancing gestation**.

Axial (upper line) and coronal (lower line) T2-WI of fetuses at 18 (a, e), 20+4 (b, f), 22 (c, g), and 24 (d, h) GW. Note the width of the ventricles and the thin brain parenchyma in the 18 GW fetus (a, e). Later, the thickness of the cortical mantle increases whereas the size of the ventricles decreases (b–d, f–h)(67).

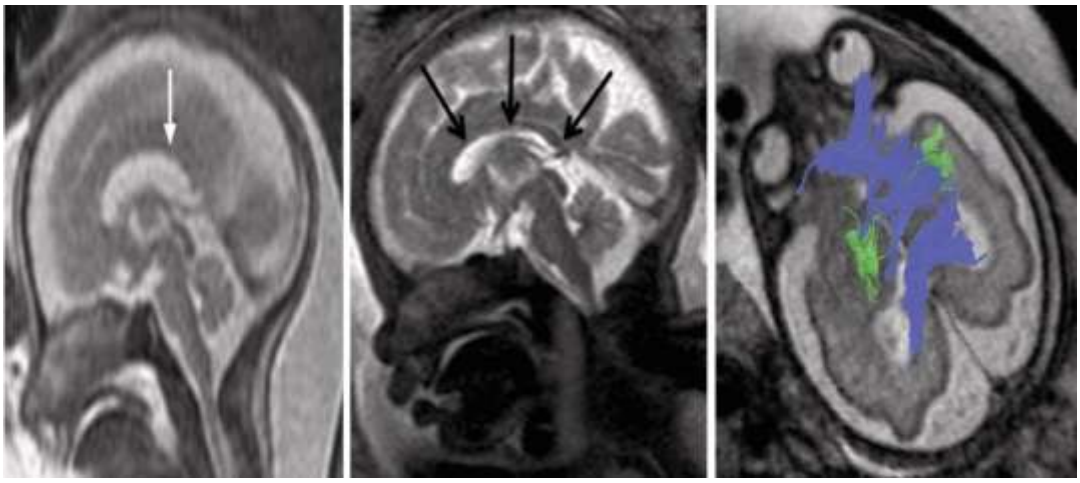

**Figure 3 Normal corpus callosum and cerebellar development**.

Sagittal T2-weighted sequence of a fetus at GW- ,32. The corpus callosum can be identified as a horizontal thin C-shaped hypointense structure (white & black arrows). (b) Diffusion tensor imaging with fiber-tracking at 28+2 GW can be used to demonstrate callosal fibers and trajectories.

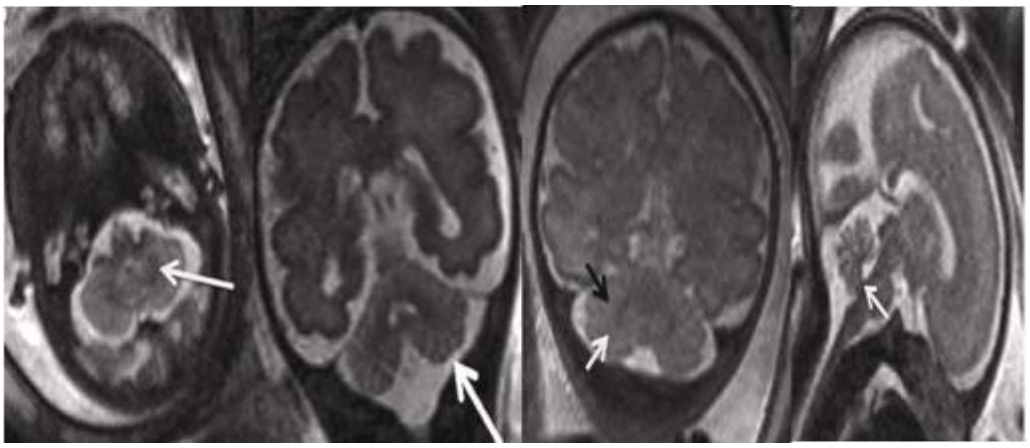

**Figure 4 Normal cerebellar development**.

The cerebellar hemispheres appear multi-layered. Axial T2-WI at 32wks GA. The gyration of the dentate nucleus shows hypointensity, hyperintense core (white arrow). Coronal T2-WI show cerebellar foliae. The cerebellar hemispheres foliae can be discriminated at 34 WKs, anterior lobe (black arrow) and posterior lobe (white arrow). Sagittal T2-WI show -flocculonodular lobe (white arrow).

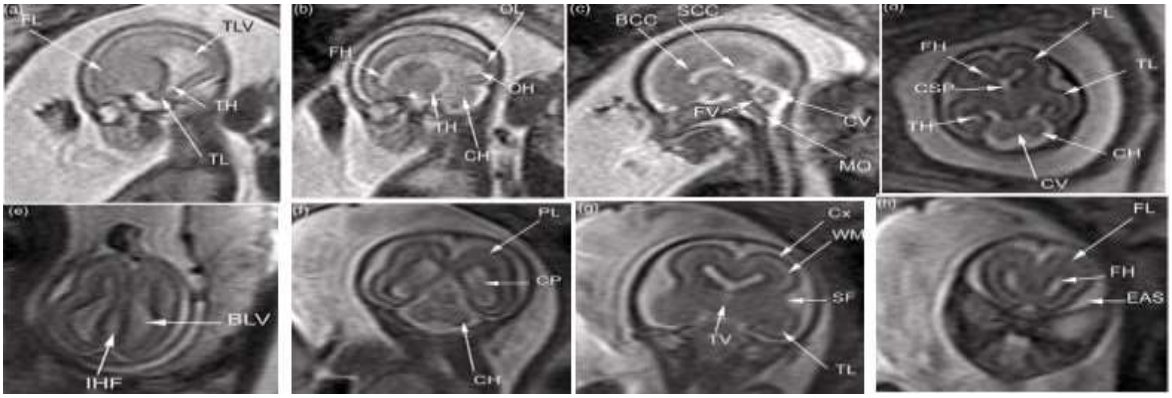


**Figure 5 Normal anatomy on T2-WI at 20 WKs GA.**

Parasagittal images (a and b) -developing frontal (FL), temporal lobes (TL). The trigone (TLV) & temporal horn (TH) lateral ventricle, occipital horn (OH), frontal horn (FH). Midline sagittal image (c) reveals the developing body (BCC) & splenium (SCC) of the corpus callosum. Posterior fossa show developing cerebellar vermis (CV) and fourth ventricle (FV), medulla oblongata (MO) of the brainstem. Axial images (d and e) show the bodies of lateral ventricles (BLV) and interhemispheric fissure (IHF). Coronal images (f–h) development of the Sylvian fissures (SF). The cavum of the septum pellucidum (CSP) lies between the frontal horns of the lateral ventricles and above the third ventricle (TV). Extra-axial cerebrospinal fluid spaces (EAS) (OL, occipital lobe; CH, cerebellar hemisphere; PL, parietal lobe; CP, choroid plexus; WM, white matter; Cx, cortex.)

## CLASSIFICATION, PATHOGENESIS AND IMAGING FEATURES OF VARIOUS CNS FETAL ANOMALIES

| GESTATIONAL AGE | STAGE/ETIOLOGY | MALFORMATIONS |
|---|---|---|
| 3-4 WKS | Dorsal induction | Anencephaly<br>Cephalocele<br>Chairi II malformation |
| 5-8 WKS | Ventral induction | Porencephalies<br>Septo-optic dysplasia<br>Pituitary maldevelopment<br>Posterior fossa malformation |
| 2-5 MONTHS | Neuronal proliferation | Microcephaly<br>Megalencephaly<br>Hemimegalencephaly<br>Neurocutaneous syndromes |
| 2-5 MONTHS | Neuronal migration | Schizencepahly<br>Lissencephaly<br>Heterotopias<br>Polymicrogyria |
| 6 MONTHS TO POSTNATAL & ADULT | Maturation & dysmyelinating disorders | Metabolic disorders<br>Toxic effects<br>Encephaloclastic disorders |

## CNS ANOMALIES

### Dandy Walker Variant

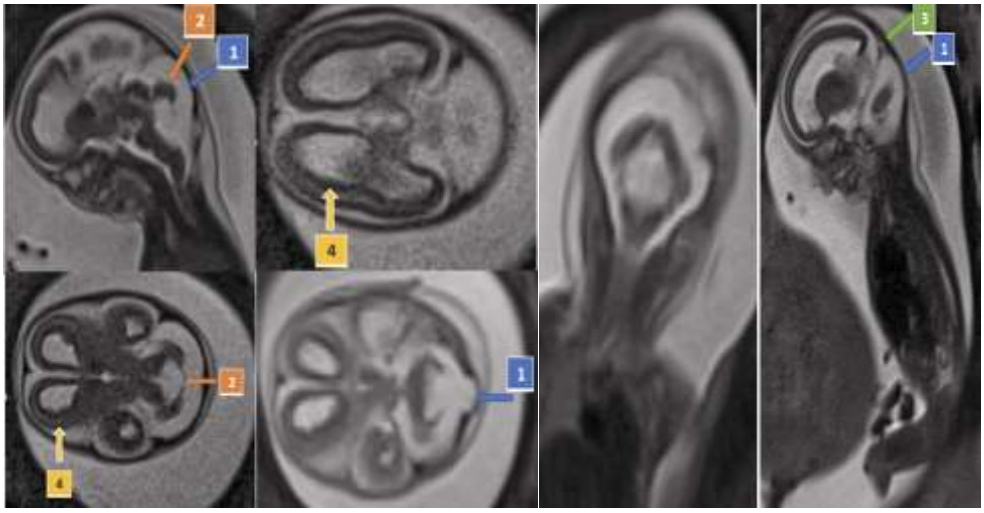

**Figure 6** Mid-sagittal and axial T2-weighted images demonstrate a large retrocerebellar cyst (1)communicating with the fourth ventricle, hypoplasia of the cerebellar vermis and hemispheres (2), enlarged posterior fossa, Torculi herophili is lying at higher level than lambdoid(3), and associated hydrocephalus(4), consistent with Dandy–Walker variant.

**Agenesis of corpus callosum with colpocephaly**

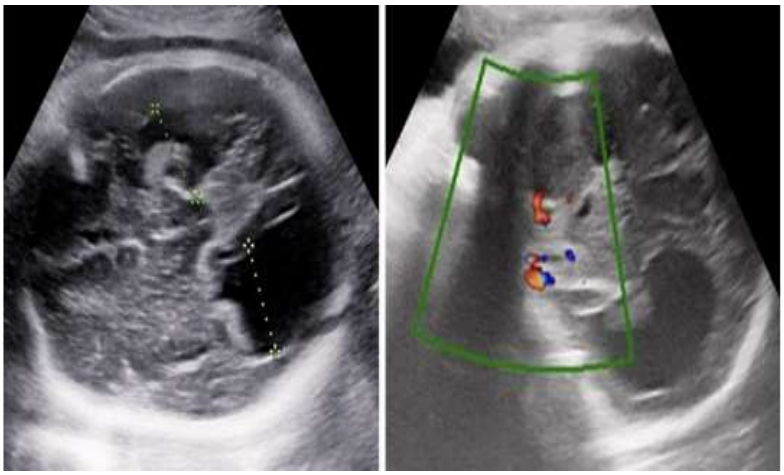

**USG shows A] Asymmetrical dilatation of bilateral lateral ventricles (predominantly occipital horns) – Colpocephaly. B] On color doppler abnormal course of pericallosal arteries.**

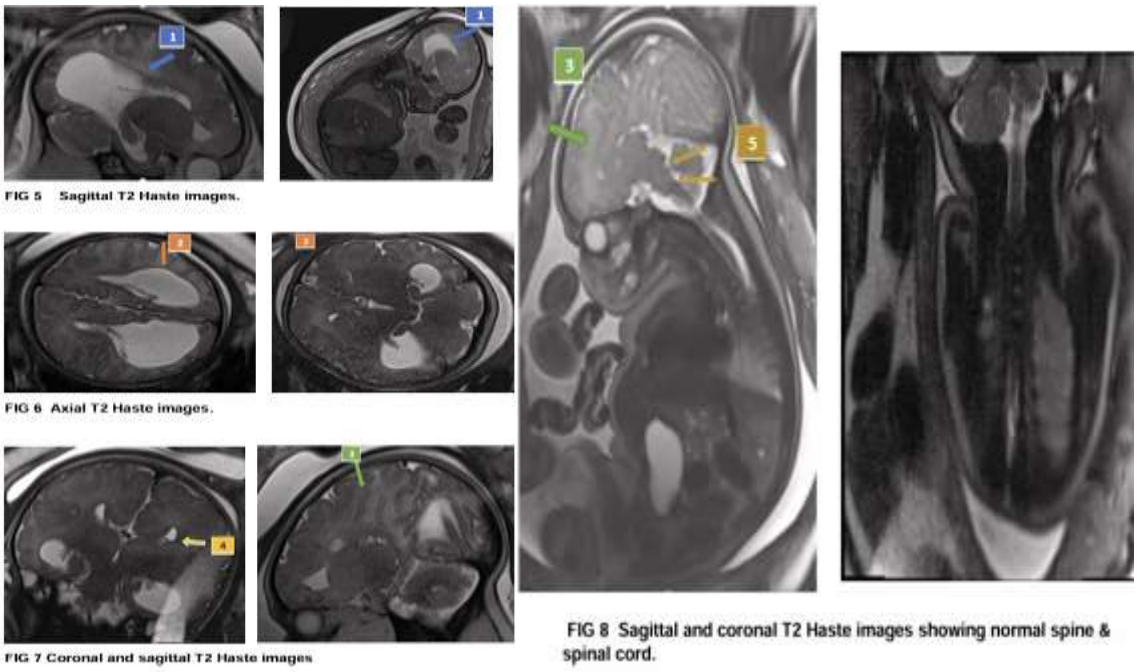


**Figure 7 Agenesis of the corpus callosum with colpocephaly.**

Axial and coronal T2-weighted images demonstrate non-visualization of the corpus callosum with disproportionate dilatation of the occipital horns of the lateral ventricles (colpocephaly), parallel orientation of the ventricles, and radial arrangement of gyri producing a “sunburst” appearance.

1. Corpus callosum not visualised.
2. “Racing car sign” and “Tear drop” appearance of bilateral lateral ventricles - Colpocephaly
3. Gyri appear radiating giving “sunray appearance”
4. Moose head/viking helmet appearance on coronal images

**Large occipital encephalocele**

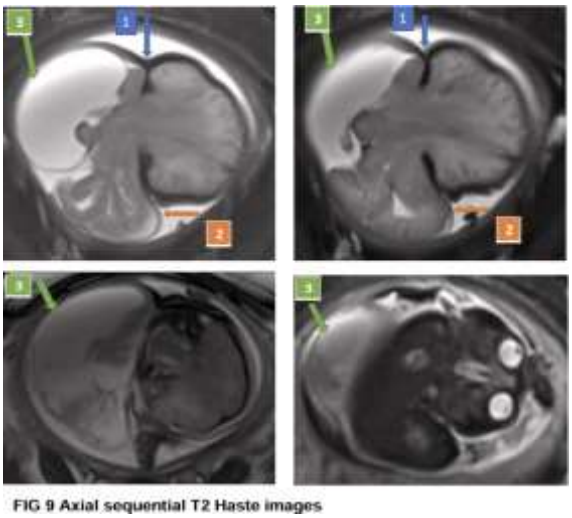


**Figure 8. Large occipital encephalocele.**

Sagittal and axial T2-weighted images show a large defect in the occipital calvarium with herniation of cerebral parenchyma and cerebrospinal fluid–filled sac containing occipital and cerebellar tissue.

1. Large defect in occipital region of fetal head
2. Cerebral parenchyma herniates, The herniated sac contain parietal, occipital lobe, cerebellum.
3. Well defined cystic lesion following CSF intensity noted in hernia sac.

**Intracranial infection [most likely cytomegalovirus/ CMV infection]**

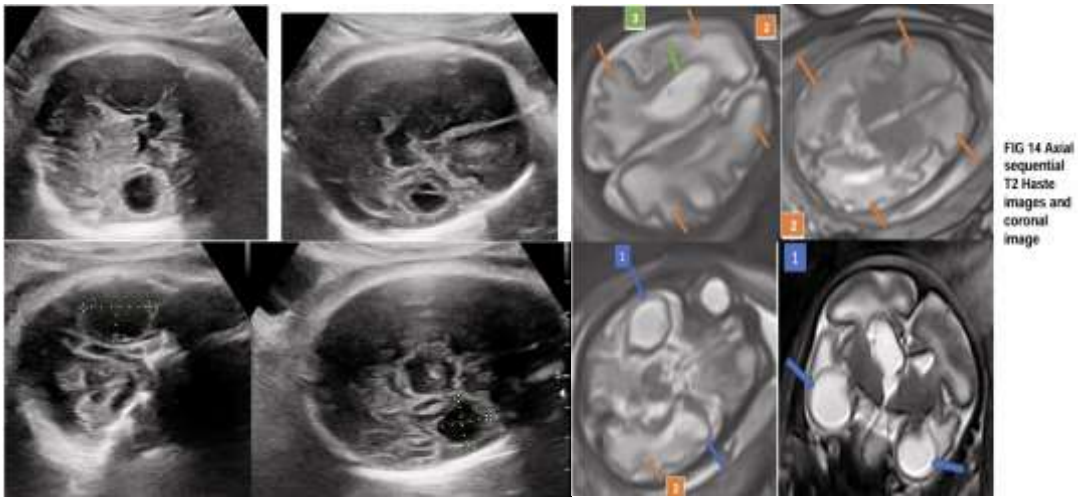


**Figure 9 Findings suggestive of congenital intracranial infection.**

Axial T2-weighted images demonstrate multiple rounded cystic lesions in the bilateral temporal lobes (1), some showing porencephalic communication, along with periventricular white matter hyperintensity(2) and mild ventriculomegaly (3), suggestive of intrauterine infection.

**Chiari malformation type II**

Fig 24 USG shows dilated bilateral lateral ventricles, complete fusion of bilateral thalami- semilobar holoprosencephaly (white arrows)

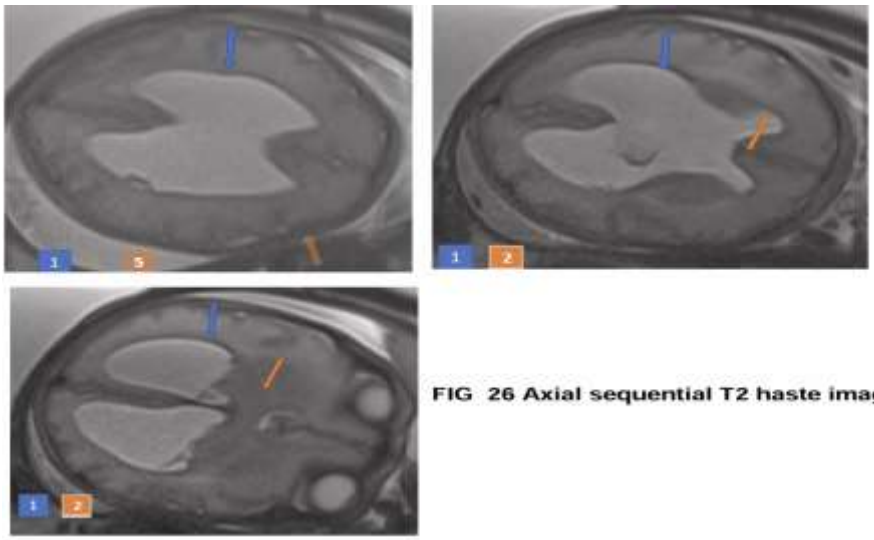

FIG 26 Axial sequential T2 haste images

**Figure 10 Chiari II malformation with associated anomalies.**

Sagittal and axial T2-weighted images demonstrate small posterior fossa, downward herniation of cerebellar tonsils, hydrocephalus, and associated spinal dysraphism. Additional systemic anomalies include kyphoscoliosis and renal fusion anomaly.

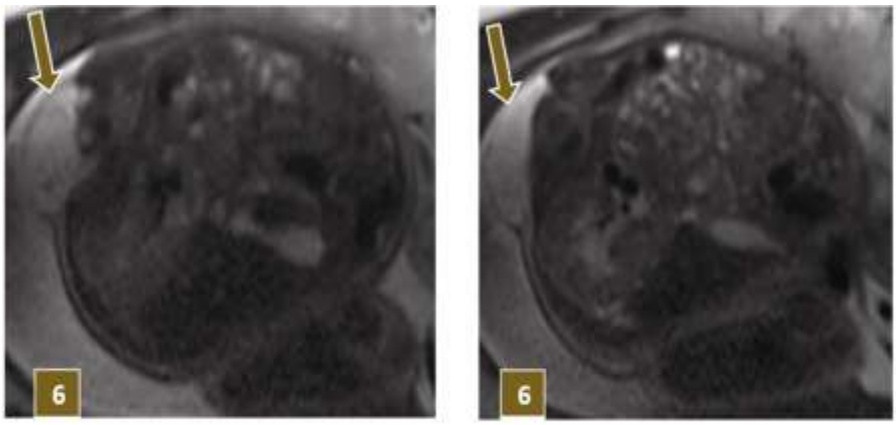


FIG 27 Axial T2 Haste images show Meningocele.

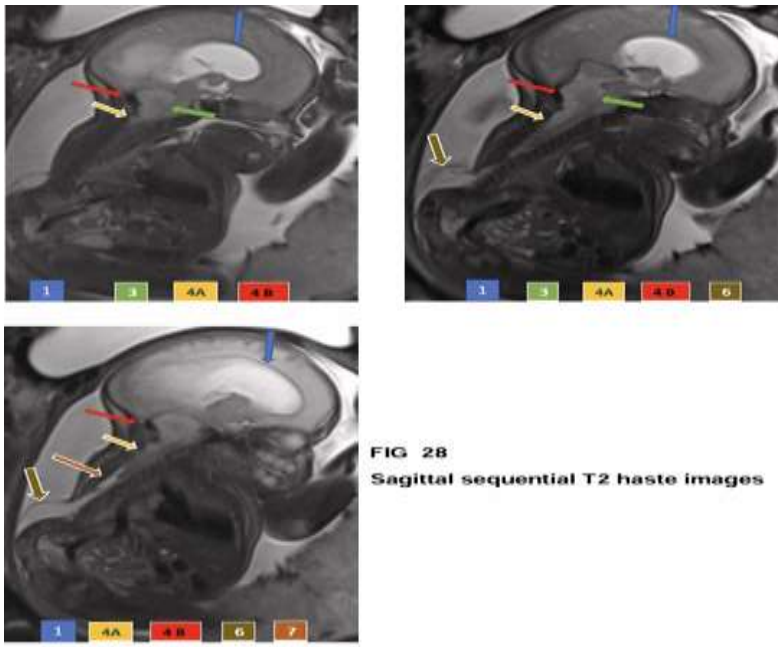

FIG 28
Sagittal sequential T2 haste images

1. Gross hydrocephalus,
2. Complete fusion of bilateral thalami- Semilobar holoprosencephaly,
3. Aqueductal stenosis,
4. Bilateral tonsillar herniation [4A] and small posterior fossa [4B],
5. Lemonhead appearance, 6) Meningocele,
6. Kyphoscoliotic , Short spine with syrinx ,
7. Cross fused **ectopic kidney, 9) Bilateral club foot.**

**TWIN GESTATION**

- **FETUS-1 is Normal**
- **FETUS -2**

1. **Spina bifida with meningomyelocele in lumbosacral region**
2. **Kyphoscoliosis in thorax**

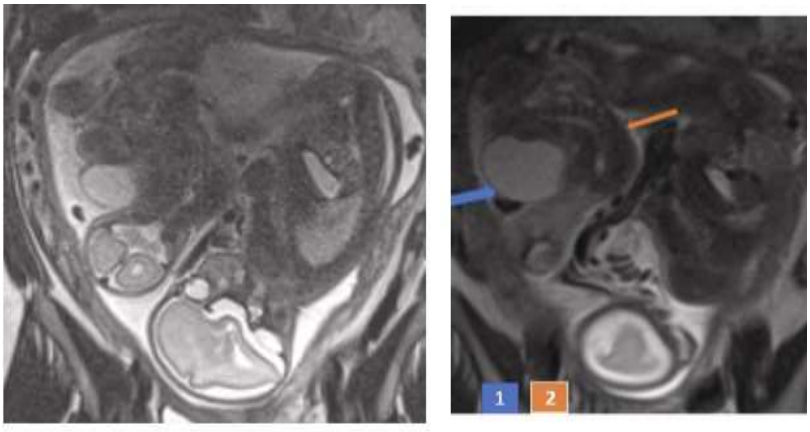

FIG 33 T2 Haste images show Twin gestation with fetus- 1 appears normal and fetus-2 shows Spina bifida with meningomyelocele in lumbosacral region with kyphoscoliosis.

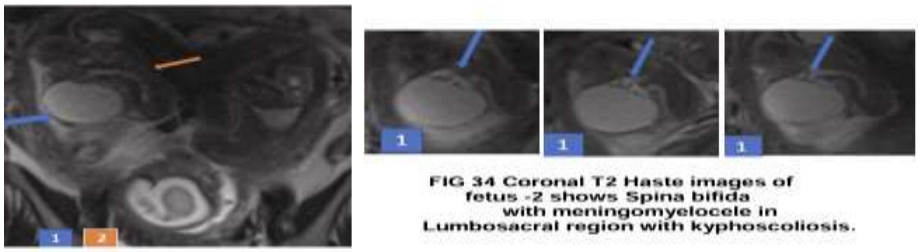

FIG 34 Coronal T2 Haste images of fetus -2 shows Spina bifida with meningomyelocele in Lumbosacral region with kyphoscoliosis.

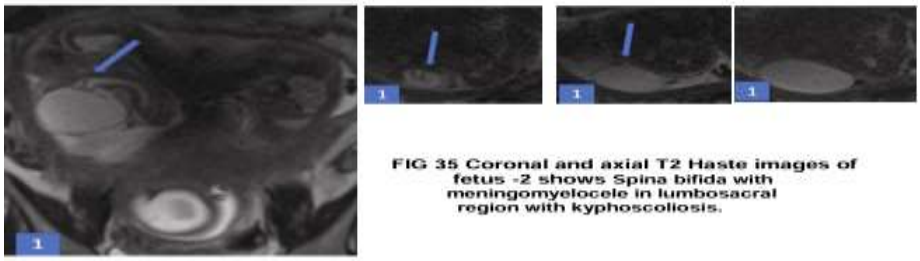

FIG 35 Coronal and axial T2 Haste images of fetus -2 shows Spina bifida with meningomyelocele in lumbosacral region with kyphoscoliosis.

## THORACIC ANOMALIES

### Congenital high airway obstruction syndrome (CHAOS SYNDROME)

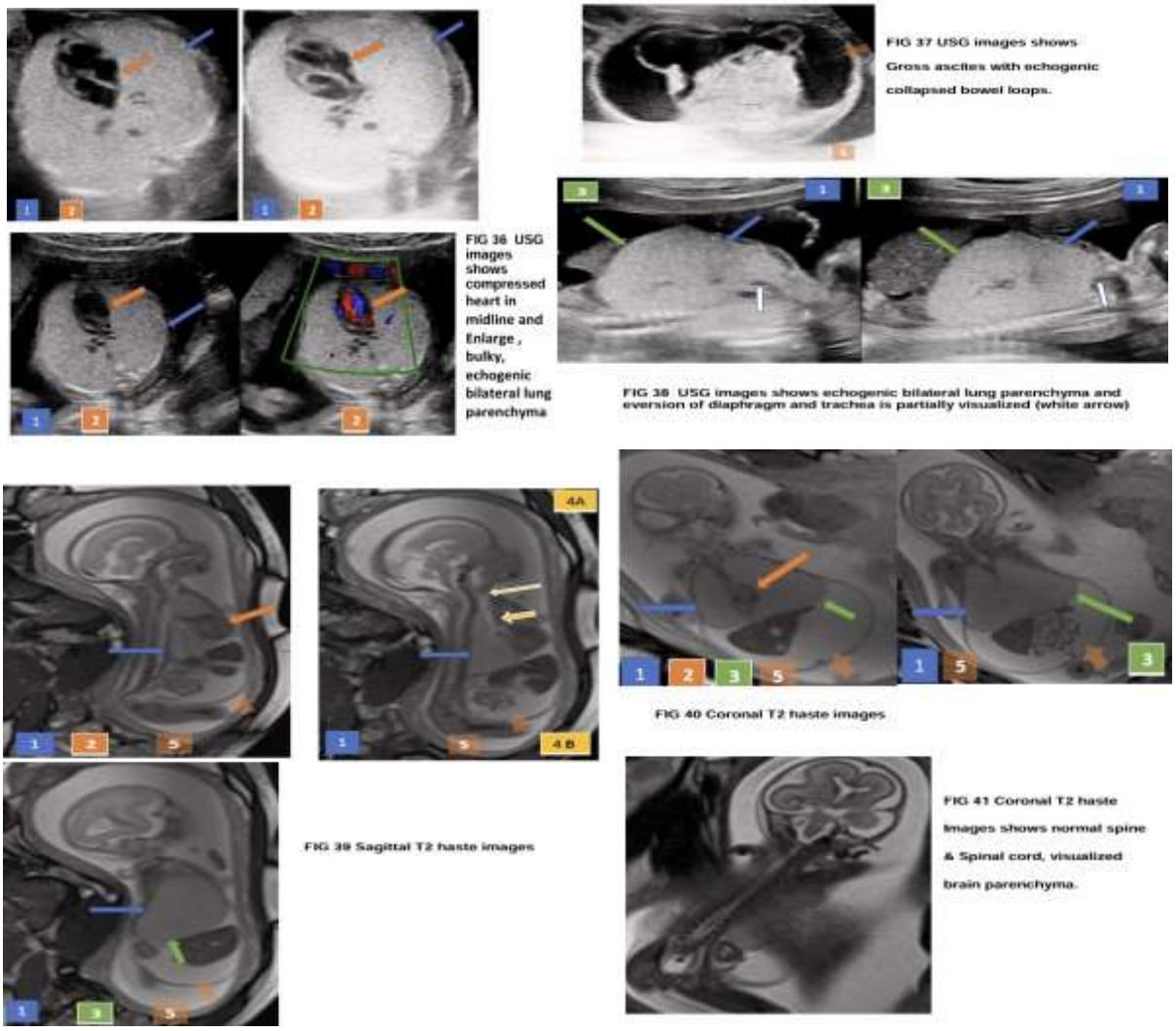


**Figure 11 Thoracic anomaly – Congenital high airway obstruction syndrome (CHAOS).**

Axial and sagittal T2-weighted images show markedly enlarged, hyperintense lungs with flattened and everted diaphragms (1,3), compressed centrally located heart(2), dilated fluid-filled trachea (4B) proximal to the obstruction (4A), and associated fetal ascites (2).

**Macrocystic CPAM (Type I – Congenital pulmonary airway malformation)**

1) Large cystic lesion in left hemithorax
2) Fetal ascites
3) Fetal hydrops
4) Gross polyhydramnios.

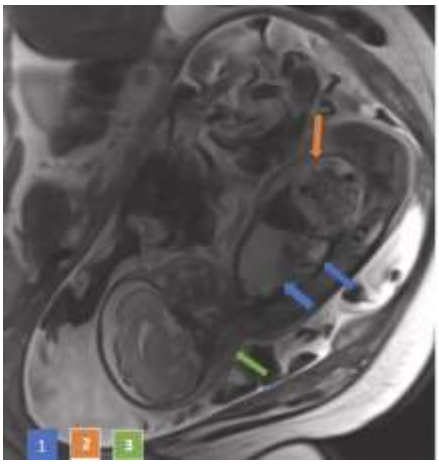

FIG 43 T2 Haste image showing gross polyhydramnios with Flow void artefacts In some sections.

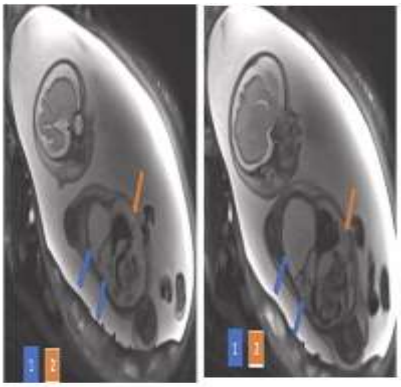

FIG 44 Sagital T2 Haste images

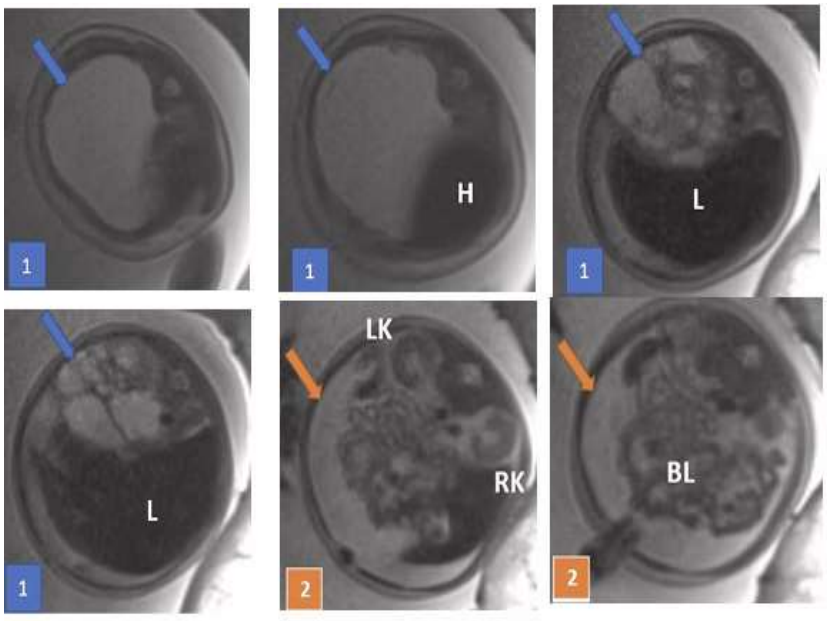


FIG 45 Axial sequential T2 HASTE images , H-heart, L-liver, RK-Right kidney , LK – Left kidney, BL- Bowel loops.

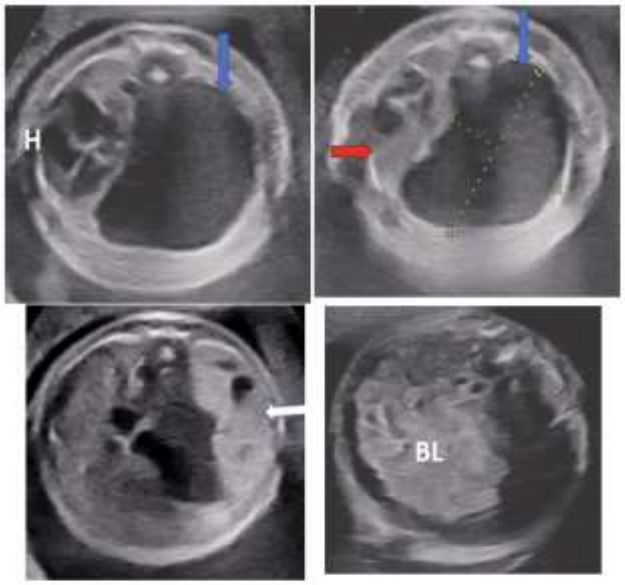


FIG 47 USG images show large cystic structure in left hemithorax, significant mediastinal shift with heart (H) and right lung collapsed (red arrow); collapsed echogenic left lung (white arrow), BL- bowel loops with ascites.

**Figure 12 Congenital pulmonary airway malformation (CPAM).**

Axial T2-weighted images demonstrate a large macrocystic lesion occupying the left hemithorax with associated mediastinal shift, fetal ascites, and features of hydrops fetalis.

**Congenital diaphragmatic hernia**

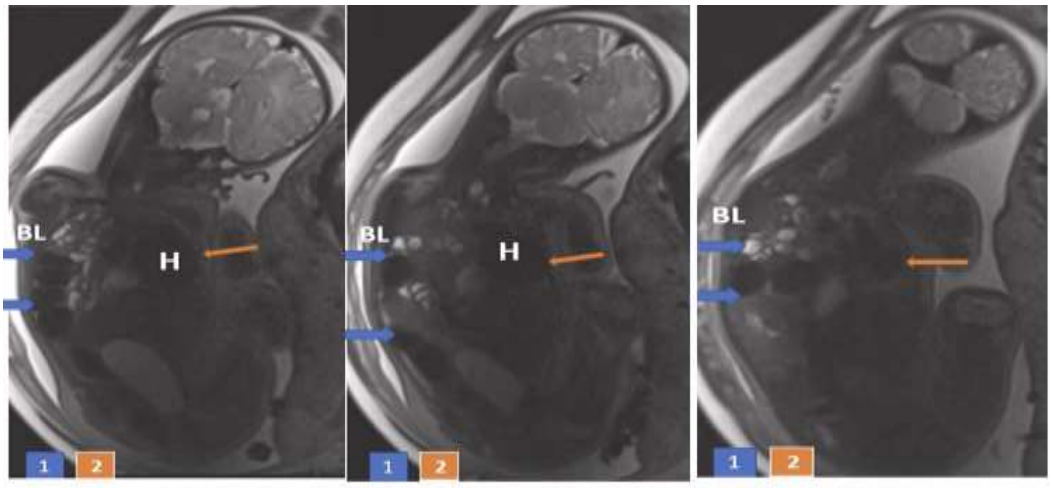


FIG 51 Coronal Sequential T2 Haste images , H- heart , BL- bowel loops.

**Figure 13 Congenital diaphragmatic hernia.**

Axial T2-weighted images demonstrate herniation of stomach and bowel loops into the left hemithorax through a posterolateral diaphragmatic defect (1), with **mediastinal** shift and ipsilateral lung hypoplasia (2).

## UROGENITAL ANOMALIES

### Multicystic dysplastic bilateral kidney

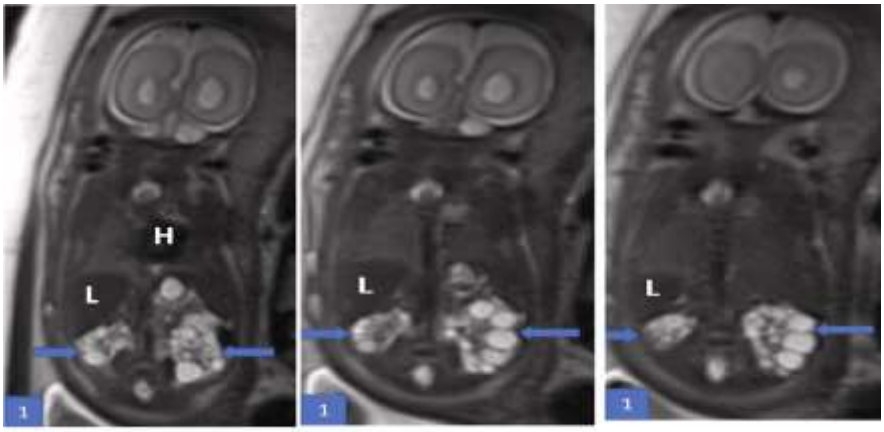


FIG 55 Coronal sequential T2 Haste images , L-liver, H- heart

**Figure 14 Bilateral multicystic dysplastic kidneys.**

Coronal and axial T2-weighted images demonstrate enlarged kidneys replaced by multiple non-communicating cysts, non-visualization of the urinary bladder, and associated severe oligohydramnios.

### Bilateral renal and Urinary bladder agenesis

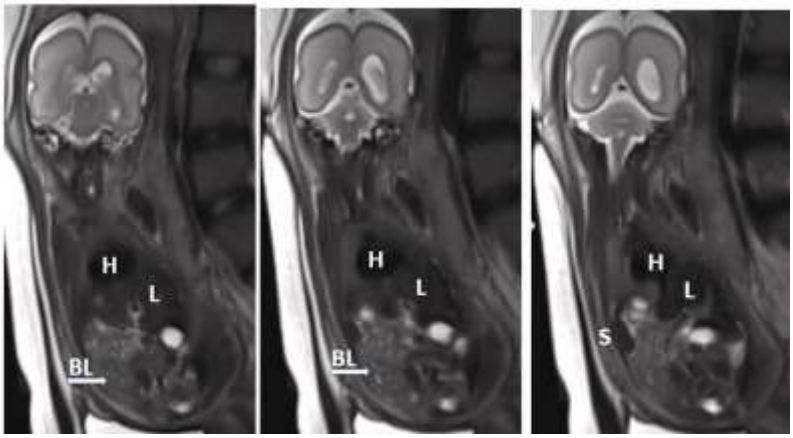


**Figure 15 Bilateral renal and urinary bladder agenesis**

1. Non visualisation of bilateral kidney – Renal agenesis.
2. Non visualisation of Urinary bladder
3. Situs Inversus with Levocardia
4. Severe oligohydramnios

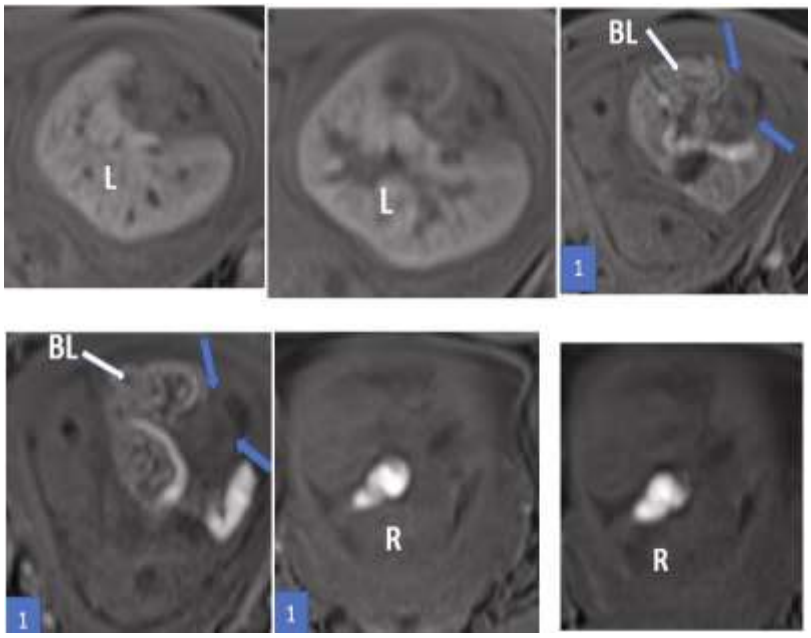


**Axial sequential T1 DIXON VIBE WATER ONLY images show , Non visualization of both kidneys in renal fossa (blue arrow) & urinary bladder in pelvis ; BL – bowel loops are collapse (white arrow) and R- Rectum shows hyperintense meconium within it.**

**Urinary bladder outlet obstruction – likely due to PUV (Posterior urethral valve)**

1. Gross hydronephrosis
2. Gross hydroureter
3. Grossly distended Urinary bladder – Bladder outlet obstruction – likely due to PUV (Posterior urethral valve)
4. Polyhydramnios

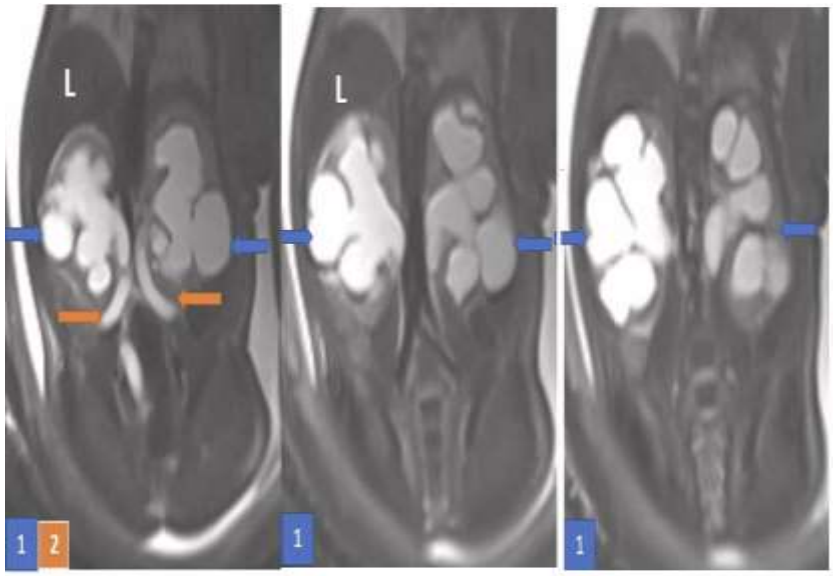

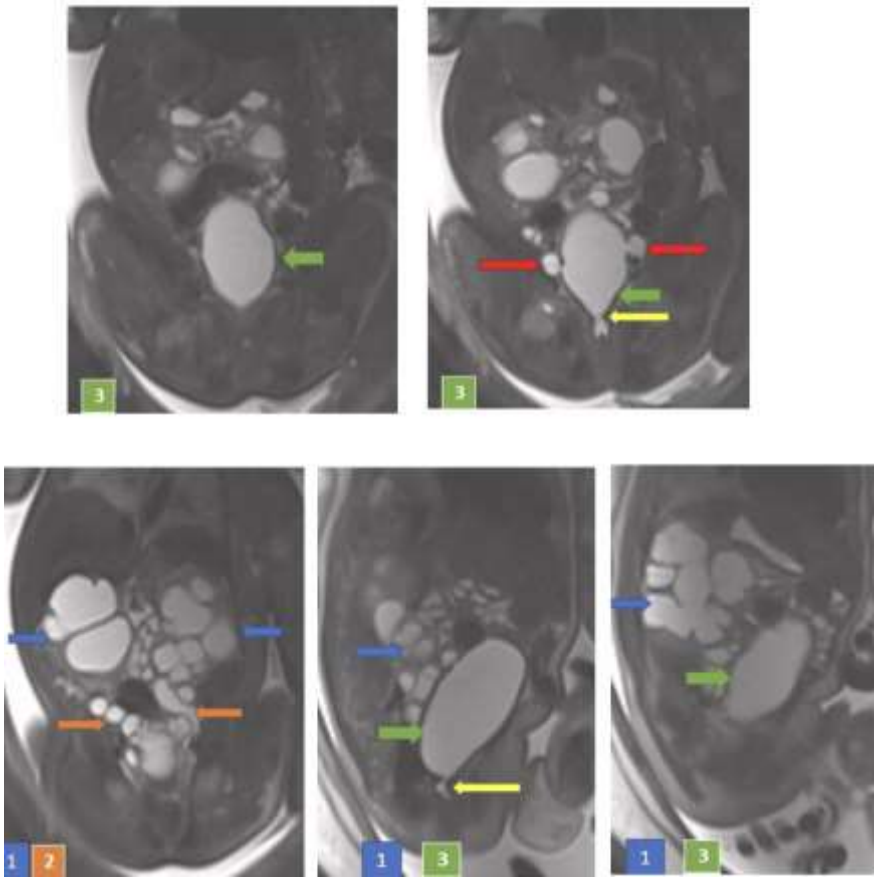

**Figure 16 Posterior urethral valve causing urinary bladder outlet obstruction.**

Coronal and sagittal T2 Haste images show bilateral gross hydronephrosis (blue arrow) & hydroureter (orange arrow); grossly distended urinary bladder , bilateral VUJ with dilated distal ureter (red arrows), Narrowed urethra with keyhole appearance (yellow arrow) – likely PUV (posterior urethral valve) causing urinary bladder outlet obstruction.

**PLACENTAL ANOMALIES**

**PLACENTA PREVIA WITH ACRETA PERCRETA SPECTRUM:**

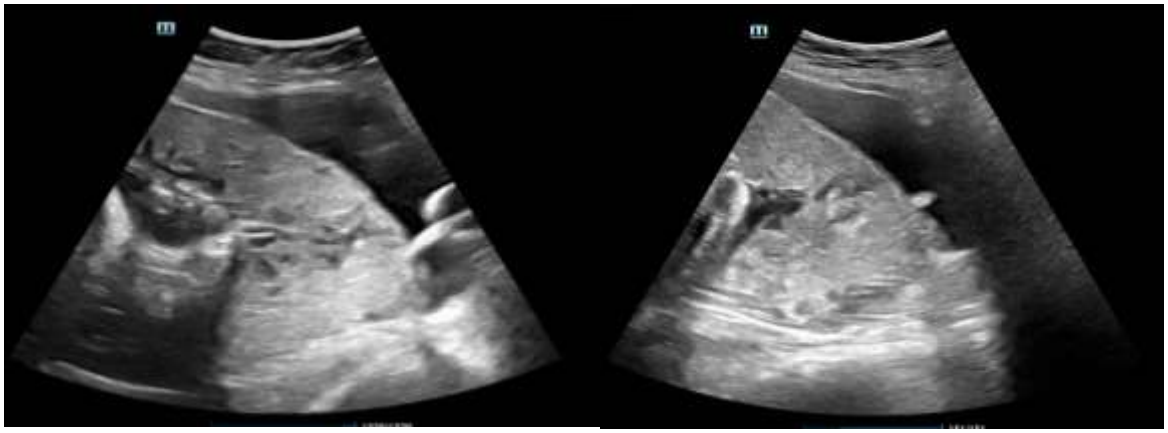

**USG Findings: Complete placenta previa covering the internal os**
**Severe myometrial thinning.**

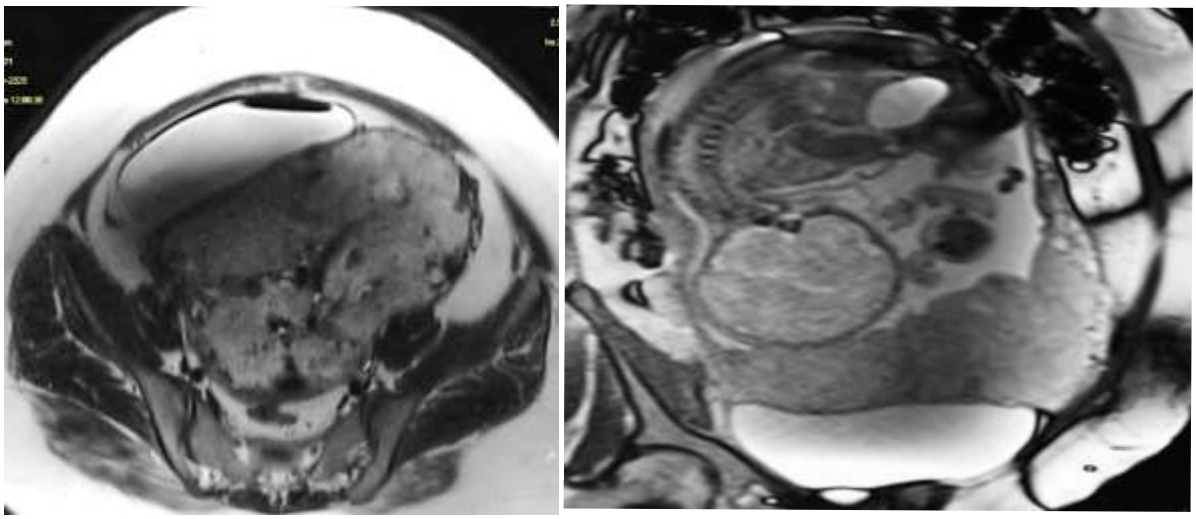

**Figure 17 Axial, Coronal and sagittal T2 Haste images show heterogeneous placenta completely covering the os with T2 hypointense bands.**
**Thinning of retroplacental zone and myometrial bladder interface.**

**COMPLETE PLACENTA PREVIA:**

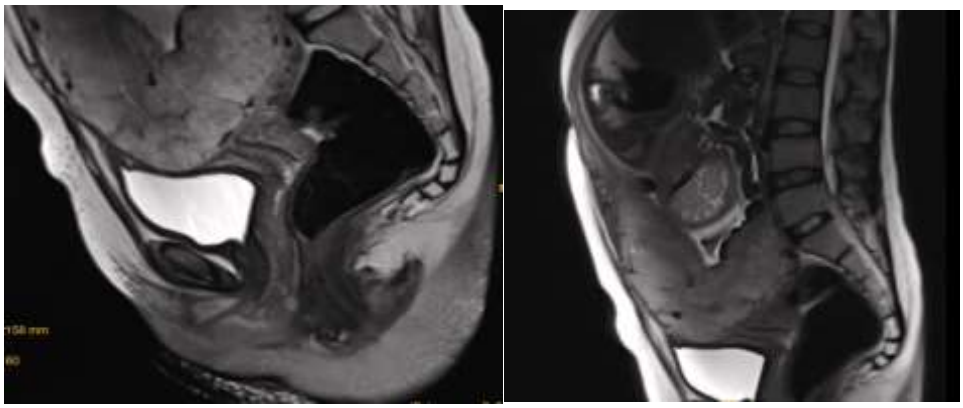

**Figure 18 Sagittal T2WI images show placenta completely covering the os.**

**PLACENTAL CHORANGIOMA:**

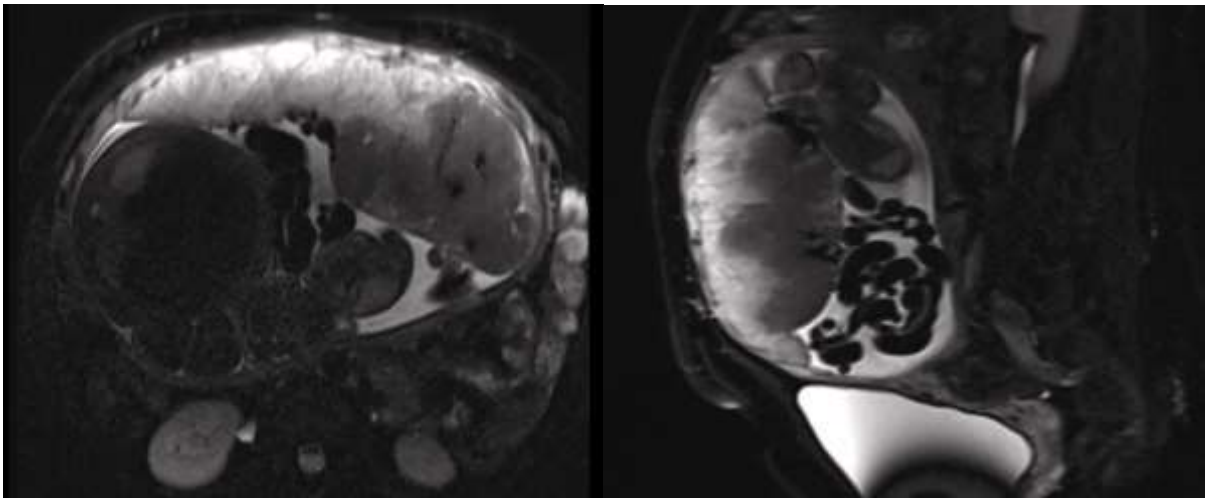

**Figure 19 Axial and sagittal T2 Haste images show well defined lobulated placental mass arising from fetal surface near cord insertion.**

**Discussion**

Prenatal magnetic resonance imaging (MRI) has become an indispensable adjunct to ultrasonography (USG) in the evaluation of complex fetal and placental abnormalities. While USG remains the primary screening modality due to its real-time capability and accessibility, its diagnostic performance may be limited by maternal obesity, oligohydramnios, unfavorable fetal position, and advanced gestational age. The present study demonstrates the added value of fetal MRI in improving diagnostic confidence and comprehensive anatomical characterization across multiple fetal organ systems.

This study is limited by its retrospective design, referral bias, and lack of uniform postnatal confirmation of findings. Additionally, sensitivity and specificity analysis could not be performed due to absence of a gold standard reference in all cases.

Central nervous system (CNS) anomalies constituted the most frequently detected abnormalities in our cohort, accounting for nearly half of the abnormal cases. MRI offered superior visualization of cortical maturation, sulcation patterns, posterior fossa structures, and midline commissural development. Conditions such as agenesis of the corpus callosum, Dandy–Walker spectrum, Chiari II malformation, and intracranial infections were more accurately delineated on MRI compared to ultrasound. The ability of MRI to demonstrate multilayered cortical architecture, commissural absence, and associated malformations was particularly useful in refining diagnoses and identifying multisystem involvement. These findings align with existing literature that emphasizes MRI's role in fetal neuroimaging, especially for evaluating complex brain malformations and prognostication.

Thoracic anomalies formed another important diagnostic group in this study. MRI enabled detailed assessment of lung parenchymal signal characteristics, airway patency, mediastinal displacement, and diaphragmatic integrity. In cases of congenital high airway obstruction syndrome (CHAOS), MRI precisely localized the level of obstruction and demonstrated secondary effects such as lung hyperexpansion, diaphragmatic eversion, and fetal hydrops. This information is critical for prenatal counseling and delivery planning, including the consideration of ex utero intrapartum treatment (EXIT) procedures. Similarly, in congenital pulmonary airway malformations and congenital diaphragmatic hernia, MRI allowed accurate evaluation of lesion extent, herniated abdominal contents, lung hypoplasia, and mediastinal shift, which are key determinants of postnatal outcome.

Genitourinary anomalies represented the second most common group in our series. MRI proved particularly valuable in cases complicated by severe oligohydramnios, where sonographic evaluation is often suboptimal. Multicystic dysplastic kidneys, renal agenesis, and urinary bladder outlet obstruction were reliably identified and characterized. The visualization of dilated urinary tracts, bladder distension, bowel meconium, and associated anomalies facilitated accurate differentiation between obstructive and non-obstructive pathologies. Identification of posterior urethral valve–related obstruction and its secondary effects allowed improved prognostication and informed parental counseling.

Placental abnormalities were effectively assessed using fetal MRI, highlighting its growing role beyond fetal anomaly detection. MRI demonstrated characteristic findings of placenta previa and placenta accreta spectrum disorders, including heterogeneous placental signal intensity, intraplacental T2 hypointense bands, thinning or loss of the retroplacental clear zone, and disruption of the uterine–bladder interface. Early and accurate diagnosis of these conditions is essential for obstetric planning, minimizing maternal morbidity, and ensuring multidisciplinary surgical preparedness. Additionally, placental chorioangiomas were well visualized as lobulated placental masses arising from the fetal

surface, aiding differentiation from other placental lesions and assessment of potential fetal complications.

Despite its diagnostic advantages, fetal MRI has certain limitations. Fetal motion can introduce artifacts, and the technique lacks the real-time assessment and Doppler capabilities of ultrasonography. Limited availability, higher cost, and the need for specialized expertise may also restrict widespread use. Furthermore, the retrospective design of this study and the absence of uniform postnatal or pathological confirmation in all cases represent limitations. Prospective studies with standardized outcome correlation and quantitative evaluation of diagnostic impact would further strengthen the evidence supporting routine use of fetal MRI in selected indications.

In conclusion, fetal MRI serves as a valuable complementary imaging modality to ultrasonography, particularly in the evaluation of complex CNS, thoracic, genitourinary, and placental abnormalities. By providing superior soft-tissue contrast and comprehensive anatomical detail, fetal MRI enhances diagnostic accuracy, facilitates informed prenatal counseling, and plays a crucial role in perinatal and postnatal management planning.

**Conclusion:**

Fetal MRI plays a vital role in the detailed evaluation of fetal and placental anomalies, especially when ultrasound findings are inconclusive or complex. This retrospective study highlights the prevalence of CNS and genitourinary anomalies as the most commonly detected conditions and underscores the importance of fetal MRI in comprehensive prenatal diagnosis and perinatal planning.

**References**

1. Levine D. Ultrasound versus magnetic resonance imaging in fetal evaluation. Top Magn Reson Imaging. 2001;12:25–38. doi: 10.1097/00002142-200102000-00004. [DOI] [PubMed] [Google Scholar]
2. Simon E.M., Goldstein R.B., Coakley F.V., Filly R.A., Broderick K.C., Musci T.J. Fast MR imaging of fetal CNS anomalies in utero. AJNR Am J Neuroradiol. 2000;21:1688–1698. [PMC free article] [PubMed] [Google Scholar]
3. Frates M., Kumar A., Benson C., Ward V., Tempany C. Fetal anomalies: comparison of MR imaging and US for diagnosis. Radiology. 2004;232:398–404. doi: 10.1148/radiol.2322030504. [DOI] [PubMed] [Google Scholar]
4. Miller E., Ben-Sira L., Constantini S., Beni-Adani L. Impact of prenatal magnetic resonance imaging on postnatal neurosurgical treatment. J Neurosurg. 2006;105(3 Suppl):203–209. doi: 10.3171/ped.2006.105.3.203. [DOI] [PubMed] [Google Scholar]
5. American College of Radiology (ACR), Society for Pediatric Radiology (SPR). ACR-SPR practice guideline for the safe and optimal performance of fetal magnetic resonance imaging (MRI). [online publication]. Reston (VA): American College of Radiology (ACR); 2010. p. 10 [cited 2010 October 1] Available from: <http://www.guidelines.gov/content.aspx?id=32509>.
6. Stecco A., Saponaro A., Carriero A. Patient safety issues in magnetic resonance imaging: state of the art. Radiol Med. 2007;112:491–508. doi: 10.1007/s11547-007-0154-4. [DOI] [PubMed] [Google Scholar]
7. Kanal E., Borgstede J.P., Barkovich A.J., Bradley W.G., Etheridge S., Felmlee J.P. American college of radiology white paper on MR safety. AJR Am J Roentgenol. 2002;178:1335–1347. doi:

10.2214/ajr.178.6.1781335. [DOI] [PubMed] [Google Scholar]
8. Glenn O.A., Barkovich A.J. Magnetic resonance imaging of the fetal brain and spine: an increasingly important tool in prenatal diagnosis, Part 1. AJNR Am J Neuroradiol. 2006;27:1604–1611. [PMC free article] [PubMed] [Google Scholar]
9. Adzick N.S., Thom E.A., Spong C.Y., Brock J.W., 3rd, Burrows P.K., Johnson M.P. A randomized trial of prenatal versus postnatal repair of myelomeningocele. N Engl J Med. 2011;364(11):993–1004. doi: 10.1056/NEJMoa1014379. [DOI] [PMC free article] [PubMed] [Google Scholar]
10. Yamashita Y., Namimoto T., Abe Y., Takahashi M., Iwamasa J., Miyazaki MR imaging of the fetus by a HASTE sequence. AJR Am J Roentgenol. 1997;168:513–519. doi: 10.2214/ajr.168.2.9016238. [DOI] [PubMed] [Google Scholar]
11. Saleem S.N. Feasibility of magnetic resonance imaging (MRI) of the fetal heart using balanced steady-state-free-precession (SSFP) sequence along fetal body and cardiac planes. Am J Roentgenol AJR. 2008;191:1208–1215. doi: 10.2214/AJR.07.3839. [DOI] [PubMed] [Google Scholar]
12. Chung H.W., Chen C.Y., Zimmerman R.A., Lee K.W., Lee C.C., Chin SCc. T2-Weighted Fast MR imaging with true FISP versus HASTE comparative efficacy in the evaluation of normal fetal brain maturation. AJR Am J Roentgenol. 2000;275:1375–1380. doi: 10.2214/ajr.175.5.1751375. [DOI] [PubMed] [Google Scholar]
13. Girard N., Fogliarini C., Viola A., Confort-Gouny S., Le Fur Y., Viout P. MRS of normal and impaired fetal brain development. Eur J Radiol. 2006;57:217–225. doi: 10.1016/j.ejrad.2005.11.021. [DOI] [PubMed] [Google Scholar]
14. Kasprian G., Brugger P.C., Weber M., Krssak M., Krampl E., Herold C. In utero tractography of fetal white matter development. Neuroimage. 2008;43:213–224. doi: 10.1016/j.neuroimage.2008.07.026. [DOI] [PubMed] [Google Scholar]
15. Webb J.A., Thomsen H.S., Morcos S.K. The use of iodinated and gadolinium contrast media during pregnancy and lactation. Eur Radiol. 2005;15:1234–1240. doi: 10.1007/s00330-004-2583-y. [DOI] [PubMed] [Google Scholar]
16. Garel C. The role of MRI in the evaluation of the fetal brain with an emphasis on biometry, gyration and parenchyma. Pediatr Radiol. 2004;34:694–699. doi: 10.1007/s00247-004-1249-x. [DOI] [PubMed] [Google Scholar]
17. Brisse H., Fallet C., Sebag G., Nessmann C., Blot P., Hassan M. Supratentorial parenchyma in the developing fetal brain: in vitro MR study with histologic comparison. AJNR Am J Neuroradiol. 1997;18:1491–1497. [PMC free article] [PubMed] [Google Scholar]
18. Bowerman R.A., Nyberg D.A. Normal fetal anatomic survey. In: Nyberg D., McGahan J., Pretorius D., Pilu G., editors. Diagnostic imaging of fetal anomalies. Lippincott Williams & Wilkins; Philadelphia: 2003. pp. 1–30. [Google Scholar]
19. Prayer D., Brugger P.C., Nemec U., Milos R.I., Mitter C., Kasprian G. Cerebral malformations. In: Prayer D., editor. Fetal MRI. Springer-Verlag; Berlin: 2011. pp. 287–308. [Google Scholar]
20. Guibaud L. Practical approach to prenatal posterior fossa abnormalities using MRI. Pediatr Radiol. 2004;34:700–711. doi: 10.1007/s00247-004-1248-y. [DOI] [PubMed] [Google Scholar]
21. McGahan J.P., Pilu G., Nyberg D. Cerebral malformations. In: Nyberg D., McGahan J., Pretorius D., Pilu G., editors. Diagnostic imaging of fetal anomalies. Lippincott Williams & Wilkins; Philadelphia: 2003. pp. 220–290. [Google Scholar]

22. Saleem S.N., Zaki M.S. Role of magnetic resonance imaging (MRI) in prenatal diagnosis of pregnancies at risk for joubert syndrome and related cerebellar disorders (JSRD) Am J Neuroradiol AJNR. 2010;31(3):424–429. doi: 10.3174/ajnr.A1867. [DOI] [PMC free article] [PubMed] [Google Scholar]
23. Saleem S.N., Zaki M.S., Soliman N.A., Momtaz M. Prenatal MRI diagnosis of molar tooth sign at 17–18 weeks of gestation in two fetuses at risk for Joubert Syndrome and related cerebellar disorders. Neuropediatrics. 2011;42:35–38. doi: 10.1055/s-0031-1275739. [DOI] [PubMed] [Google Scholar]
24. Malinger G., Lev D., Lerman-Sagie T. The fetal cerebellum. Pitfalls in diagnosis and management. Prenat Diagn. 2009;29:372–380. doi: 10.1002/pd.2196. [DOI] [PubMed] [Google Scholar]
25. Saleem S.N., Said A.H., Abdel-Raouf M., El-Kattan E., Zaki M.S., Madkour N., Shokry M. Fetal MRI in the evaluation of fetuses referred for sonographically suspected neural tube defects (NTDs): impact on diagnosis and management decision. Neuroradiology. 2009;51(11):761–772. doi: 10.1007/s00234-009-0549-0. [DOI] [PubMed] [Google Scholar]
26. Benacerraf B., Nyberg D. The face and neck. In: Nyberg D., McGahan J., Pretorius D., Pilu G., editors. Diagnostic imaging of fetal anomalies. Lippincott Williams & Wilkins; Philadelphia: 2003. pp. 335–379. [Google Scholar]
27. Kathary N., Bulas D.I., Newman K.D., Schonberg R.L. MRI imaging of fetal neck masses with airway compromise: utility in delivery planning. Pediatr Radiol. 2001;31:727–731. doi: 10.1007/s002470100527. [DOI] [PubMed] [Google Scholar]
28. Poutamo J., Vanninen R., Partanen K., Ryynanen M., Kirkinen P. Magnetic resonance imaging supplements ultrasonographic imaging of the posterior fossa, pharynx and neck in malformed fetuses. Ultrasound Obstet Gynecol. 1999;13:327–334. doi: 10.1046/j.1469-0705.1999.13050327.x. [DOI] [PubMed] [Google Scholar]
29. Nemec S.F., Brugger P.C., Kasprian G., Nemec U., Graham J.M., Jr, Prayer D. The skeleton and musculataure. In: Prayer D., editor. Fetal MRI. Springer-Verlag; Berlin: 2011. pp. 235–246. [Google Scholar]
30. Shinmoto H., Kashima K., Yuasa Y., Tanimoto A., Morikawa Y., Ishimoto H. MR imaging of non-CNS fetal abnormalities: a pictorial essay. Radiographics. 2000;20:1227–1243. doi: 10.1148/radiographics.20.5.g00se071227. [DOI] [PubMed] [Google Scholar]